Dalton Transactions

Accepted Manuscript

ROYAL SOCIETY OF CHEMISTRY

www.rsc.org/dalton

Journal Name

ARTICLE

Synthesis, Crystal Structure, Electronic Structure, and Photoelectric Response Properties of KCu_2SbS_3†

Received 00th January 20xx,
Accepted 00th January 20xx

DOI: 10.1039/x0xx00000x

www.rsc.org/

Ruiqi Wang,[a,‡] Xian Zhang,[a,‡] Jianqiao He,[b] Chong Zheng,[c] Jianhua Lin,[a] and Fuqiang Huang*[a,b]

Copper thioantimonates have received enormous attention due to their potential for applications as photovoltaic devices. In this work, a new layered compound KCu_2SbS_3 was synthesized *via* a reactive flux method using thiourea as reactive flux. The compound crystallizes in the triclinic space group $P\bar{1}$. The structure features two-dimensional $[Cu_2SbS_3]^-$ layers stacking along the *c* axis with K^+ ion intercalated between the layers. Each $[Cu_2SbS_3]^-$ layer is composed of two single graphene-like layers connected *via* interlayer Cu–S bonds and Cu···Sb contacts. The optical measurements indicates that the compound has a band gap of 1.7 eV. Hall effect measurement shows that KCu_2SbS_3 is a p-type semiconductor with carrier concentration of 7×10^{16} cm^{-3}. First-principles calculations reveal that the direct transition occurs between Cu-3*d*-S-3*p* orbitals (VBM) to Sb-5*p*-S-3*p* orbitals (CBM). The photoelectric response properties of KCu_2SbS_3 under visible light irradiation were measured. The photocurrent is 3.7 $\mu A/cm^2$ at 10 V bias, demonstrating its potential for applications in photoelectric devices.

Introduction

Solar energy has been proved to be an alternative solution to the problems caused by conventional fossil source.[1] Compared with the first generation silicon-based solar cells, thin film solar cells should have more potential applications because they are lightweight and flexible.[2-4] Many materials have been found to function as the absorber in thin film solar cells such as CdTe,[5, 6] $CuInGaSe_2$ (CIGS)[7, 8] and Cu_2ZnSnS_4 (CZTS)[9, 10]. Recently, the copper-antimony-sulfide (CAS) system has also provided some potential materials as solar light absorbers in thin film solar cells.[11-15] Composed of sustainable and low-toxic elements, these materials establish a large absorption coefficient of over 10^5 cm^{-1} at visible light region, showing potential as alternatives for CIGS in thin film solar cells.[16]

During the past two decades, many thioantimonate have been synthesized which show abundant structural diversities.[17-24] Particularly, in the CAS system there exist various phases due to the variable valences of Cu (I or II) and Sb (III or V), different types of Cu and Sb coordination environment (CuS_n and SbS_n, n = 3, 4) and diversified modes of connection between CuS_n and SbS_n. Four major phases are known in the ternary CAS system: $CuSbS_2$ (chalcostibite), $Cu_{12}Sb_4S_{13}$ (tetrahedrite), Cu_3SbS_3 (skinnerite), and Cu_3SbS_4 (famatinite). $CuSbS_2$ consists of $[CuSbS_2]$ neutral layers packing along the *c*–axis, while the other three compounds possess 3D structures instead of layered structure. The Cu atoms adopt 4-fold CuS_4 coordination in $CuSbS_2$ and Cu_3SbS_4 while both CuS_4 and CuS_3 exist in $Cu_{12}Sb_4S_{13}$ and Cu_3SbS_3. The Sb atoms in Cu_3SbS_4 assume 4-fold coordination compared with 3-fold coordination of that in the other three ternary compounds. The band gaps of these four compounds are, respectively, 1.38 eV for $CuSbS_2$[25], 1.72 eV for $Cu_{12}Sb_4S_{13}$[16], 1.84 eV for Cu_3SbS_3[26], and 1.2 eV for Cu_3SbS_4[27]. The electronic structures of these compounds are similar which show Cu 3*d* and S 2*p* characters below the valence band maximum (VBM) and Sb 5*p* character above the conductive band minimum (CBM).[27]

In addition to these ternary compounds, some other compounds containing alkali ion (Na_2CuSbS_3,[28] K_2CuSbS_3[29]) or organic molecules ($[en]_{0.5}Cu_2SbS_3$,[30] $(C_4H_{12}N_2)_{0.5}[CuSb_6S_{10}]$,[31] $(C_2N_2H_{10})Cu_2SbS_3$,[32] $(C_6N_2H_{18})_{0.5}Cu_2SbS_3$, $(C_4N_3H_{14})Cu_3Sb_2S_5$, $(C_6N_4H_{20})_{0.5}Cu_3Sb_2S_5$[33]) have also been synthesized in the CAS system. Some of these compounds consist of layered structures which can be either neutral ($[Cu_2SbS_3]$ in $(en)_{0.5}Cu_2SbS_3$) or anionic ($[CuSbS_3]^{2-}$ in K_2CuSbS_3). Layered structures of these compounds make it possible to tune their electrical and optical properties *via* thickness-dependent quantum confinement effects construction.[34] The optical properties of some quaternary compounds and organic-inorganic hybrid compounds have been measured. K_2CuSbS_3 has an experimental indirect band gap of 2.2eV.[29]

[a] Beijing National Laboratory for Molecular Sciences and State Key Laboratory of Rare Earth Materials Chemistry and Applications, College of Chemistry and Molecular Engineering, Peking University, Beijing 100871, China. hufangfq@pku.edu.cn.
[b] CAS Key Laboratory of Materials for Energy Conversion and State Key Laboratory of High Performance Ceramics and Superfine Microstructure, Shanghai Institute of Ceramics, Chinese Academy of Sciences, Shanghai 200050, P. R. China.
[c] Department of Chemistry and Biochemistry, Northern Illinois University, DeKalb, IL 60115, USA.
‡ Ruiqi Wang and Xian Zhang contribute equally. The authors declare no competing financial interest.

† Electronic Supplementary Information (ESI) available: SEM images; EDX spectrum; the selected bond length and angle; Partial density of states of K, Cu, Sb, and S; Detailed partial DOS of the *d* orbitals of the Cu atoms. For ESI and crystallographic data in CIF format see DOI: 10.1039/x0xx00000x

$(C_2N_2H_{10})Cu_2SbS_3$ has intermediate band gaps of about 1.9 eV.[32] However, the optical absorptions of the other compounds were not reported, and photoelectric applications of these compounds have not been explored neither. Particularly, the K^+-intercalated layered compound K_2CuSbS_3 was synthesized by traditional solid state method at the high temperature of 823 K, with side products of ternary K/Sb/S and binary Cu/S species. Other compounds containing organic molecules were all synthesized under solvothermal conditions. The sulfur sources used when synthesizing these compounds were either element powder S or metal chalcogenides Cu_2S and Sb_2S_3.

Here we report a new K^+-intercalated compound KCu_2SbS_3 consisting of anionic layers $[Cu_2SbS_3]^-$. In contrast to K_2CuSbS_3, this new compound was synthesized using reactive flux method at a relatively low temperature (200°C). Thiourea was used as both the S source and flux. The relatively mild reaction condition and solution phase reaction both afford the high purity and homogeneity of the final compound. The color of KCu_2SbS_3 power is dark red, which is corresponding to its optical band gap (1.7eV). The electron structure calculation reveals a direct-bandgap semiconductor with band gap value 1.37eV for this compound. The photoelectric response property of KCu_2SbS_3 has been measured and the result shows that this material has a potential for photovoltaic application.

Experimental

Reagent

All the starting materials were obtained from Sinopharm Chemical Reagent Beijing Co., Ltd without further purifications: (i) potassium hydroxide, AR, 96%; (ii) $Cu(CH_3COO)_2{\cdot}2H_2O$, AR, 99%; (iii) antimony powder, 99.7%; (v) thiourea, AR, 99%. All the reagents are kept in a drybox prior to use.

Synthesis of KCu_2SbS_3

Single crystals of KCu_2SbS_3 were synthesized by the reactive flux method with the thiourea acting as the reactive flux. Reactants including Sb powder (0.3044 g, 2.5 mmol), $Cu(CH_3COO)_2{\cdot}2H_2O$ (0.9982 g, 5 mmol), KOH (10 g) and thiourea (8 g) were mixed directly then added into a 25ml Teflon-lined stainless steel autoclave. The reaction process was carried out under autogenous pressure at 200°C for 3 days. At this temperature thiourea would melt and act as solvent. After the autoclave was cooled down to room temperature, the product was taken out and washed with cool deionized water. The final product was collected and dried in an oven at 80°C for 6 h.

Single Crystal X-ray Crystallography

A single crystal suitable for X-ray diffraction was chosen, while the data collection was performed on an *Agilent Super Nova Diffractometer* equipped with mirror-monochromated Mo K_α radiation. The structure of KCu_2SbS_3 was solved by direct methods and refined by full-matrix least-squares techniques on F^2 by using the SHELXTL program package.[35] The crystal data and refinement details are summarized in Table 1 and selected interatomic distances and bond angles are presented in Table S1 in ESI.

Powder X-ray Diffractions

The as-synthesized crystalline sample was ground into fine powder before use. Phase purity of the powder sample was checked by powder X-ray diffraction, which was performed on a *Bruker D2 phaser* diffractometer equipped with a monochromatized source of Cu K_α radiation (λ = 0.15406 nm) at 4 kW (40 kV, 100 mA). The patterns were recorded in a slow- scanning mode with 2θ from 5° to 80° with a scan-rate of 1.2°/min. Simulated patterns were generated by using the *CrystalMaker* program and the CIF file of the refined single crystal structure.

Table 1. Crystallographic data and details of the structure refinement for KCu_2SbS_3

formula	KCu_2SbS_3
F_w (g·mol^{-1})	384.14
crystal system	triclinic
space group	$P\bar{1}$
a (Å)	6.3809(4)
b (Å)	9.1331(5)
c (Å)	10.4627(5)
α (deg)	90.501(2)
β (deg)	91.361(2)
γ (deg)	91.477(2)
V(Å^3)	609.35(3)
crystal color	black
ρ_c (g·cm^{-3})	4.187
μ (mm^{-1})	12.883
F(000)	704
R_{int}	0.0509
$R1[I>2\sigma(I)]$	0.0179
wR_2 (all data)	0.0392
GOF	1.075

Solid-state UV-Vis-NIR Spectroscopy

The solid-state ultraviolet-visible-near-infrared (UV-Vis-NIR) light diffuse-reflectance spectra of the fine powder of KCu_2SbS_3 were measured on a UV−4100 spectrophotometer operating from 1500 nm to 400 nm at room temperature. The fine powder of the as-synthesized sample was spread on a compacted base of $BaSO_4$ powder (100% reflectance standard). The generated reflectance-versus-wavelength data were used to measure the band gap of the as-synthesized samples. The reflectance data were converted to absorbance data by using the Kubelka-Munk equation.[36, 37]

Thermal investigation

Differential scanning calorimetry (DSC) and thermogravimetry (TG) were performed using a Thermal Analysis SDT2960

thermal analyzer under nitrogen flow. Well-grinded powder sample (8 mg) was loaded into an aluminum pan placed on the sample side of the detector, and an empty aluminum pan was placed on the reference side. The sample was heated to 500 °C at 10 °C/min.

Photoelectric Properties and Hall Effect

The ceramic sample was prepared by pressing the sample powder into a pellet with a diameter of 5 mm under a pressure of 10 MPa. Then the pellet was sealed in an evacuated quartz tubes and sintered into a compacted ceramic pellet under 300°C for 5 h. Current–Voltage (*I–V*) measurements were performed by sweeping the voltage from the positive maximum to the negative minimum using a semiconductor characterization system (KEITHLEY 4200). Hall effect of the ceramic pellet of KCu_2SbS_3 was explored with the physical property measurement system (PPMS).

Electronic Structure Calculations

The first–principles computations based on density functional theory (DFT) were performed using the WIEN2K program package.[38] The Perdew-Burke-Ernzerhof (PBE)[39] version of the generalized gradient approximation (GGA) was used to describe the exchange correlation functional, and the linearized augmented plane wave (LAPW) method (PAW)[40] method was used in the present work. The atomic electron configuration treated 4s as valence state for K, 3d and 4s as valence states for Cu, 5s and 5p as valence states for Sb and 3p as valence state for S. The cutoff energy of plane wave was chosen at 350 eV. For the structure optimizations, a 6×6×6 Monkhorst-Pack grid was used for the primitive cell and a 4×4×4 k-points for the conventional cell, respectively. The relaxation of geometry optimization was performed until the total energy change was within 1×10^{-6} eV/atom and the Hellmann-Feynman force on all atomic sites was less than 0.01 eV/Å.

Results and discussion

Synthesis and Crystal Structure Description

Due to the mild reaction condition (low reaction temperature), reactive flux method can be used to synthesize metastable chalcogenides.[41, 42] Recently, thiourea has been found to be a good reactive flux because it can gradually release S when heated above its melting point (182 °C).[43,44] Here we synthesize a new compound KCu_2SbS_3 using the reactive flux (thiourea) method with the assistance of the condensed base KOH. To our knowledge this is the first thioantimonate synthesized using thiourea as reactive flux. SEM image of well-defined KCu_2SbS_3 crystal is presented in Fig. S1a in ESI. The presence of K, Cu, Sb and S was confirmed by semi-quantitative energy dispersive X-ray analysis (EDX) as shown in Fig. S1b in ESI and the average atomic radio is 1/2.5/1.4/3.1.

The KCu_2SbS_3 compound crystallizes in the triclinic space group $P\bar{1}$, it is isostructural with KCu_2BiS_3 (whose was solved by powder X-ray diffraction).[45] The structure consists of two independent K sites, four independent Cu sites, two independent Sb sites and six independent S sites. KCu_2SbS_3 is composed of negative charged $[Cu_2SbS_3]^-$ layers separated by

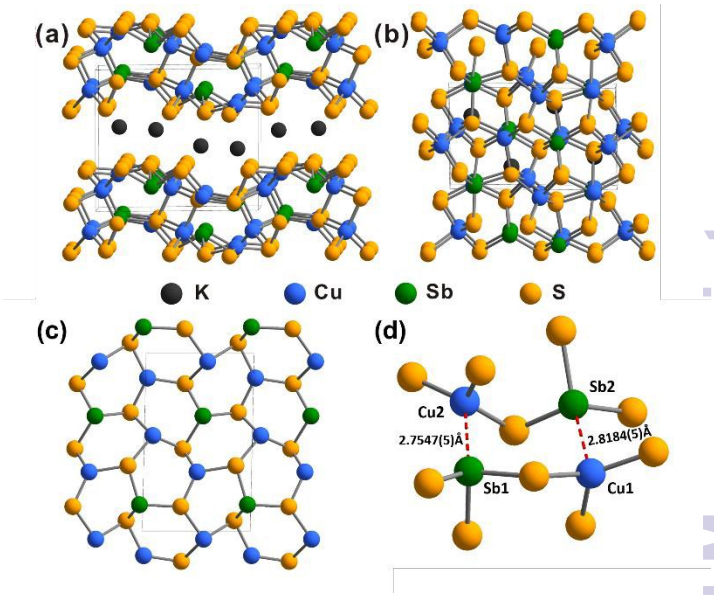

Fig. 1 Schematic diagrams of the structure of KCu_2SbS_3 viewed down the *a* axis (a) and the *b* axis (b). (c) A single layer composed by six–membered heterorings viewed down the *b* axis. (d) The coordination environment of Cu (1), Cu(2), Sb(1), and Sb(2) .

K^+ ions (Fig. 1). The layered structure of KCu_2SbS_3 is shown in Fig. 1a. Each $[Cu_2SbS_3]^-$ layer is composed of two single heavily distorted graphene-like layers as shown in Fig. 1c. The six-membered heterorings $[Cu_2SbS_3]$ are edge–sharing to form a single layer extending along the (001) plane. In the single layer, each SbS_3 is connected with six nearest CuS_3. Two single layers are combined together by the Cu(3)-S and Cu(4)-S bonds to form a 2D double-layered structure. The interactions between Sb and Cu(1, 2) also contribute to the connection of the two single layers.

There are two types of coordination of Cu atoms: i) the Cu(1) and Cu(2) sites have 3-fold coordination with S atoms to form $[CuS_3]^{5-}$ triangles; ii) the Cu(3) and Cu(4) positions possess 4-fold coordination with S atoms to form distorted $[CuS_4]^{7-}$ tetrahedra. The average Cu-S distances are 2.312 Å in $[CuS_3]^{5-}$ triangles and 2.387 Å in distorted $[CuS_4]^{7-}$ tetrahedra, respectively. The Sb atom is coordinated to three S atoms to form a $[SbS_3]^{3-}$ trigonal pyramidal motif with average Sb-S distance of 2.448 Å. It is worthy to note that the Cu···Sb distances are 2.8184(5) Å for Cu(1)···Sb(2) and 2.7547(5) Å for Cu(2)···Sb(1). The short Cu···Sb distances indicate the existence of interactions between Cu(1, 2) and Sb (Fig. 1d). I The average S–Sb–S bond angles are 100.7° for Sb(1) and 102.9° for Sb(2), which implies the presence of the stereochemically active $5s^2$ lone pair with an orientation towards Cu(1) or Cu(2). Therefore, the lone pairs are located at the fourth coordination site of Cu(1) and Cu(2).

Although a few copper thioantimonates with layered structures have been found such as $CuSbS_2$,[11] KCu_2SbS_3,[29] $(en)_{0.5}Cu_2SbS_3$,[30] $(C_2N_2H_{10})_{0.5}Cu_2SbS_3$,[32] $(C_4N_3H_{14})Cu_3Sb_2S_5$ and $(C_6N_4H_{20})_{0.5}Cu_3Sb_2S_5$,[33] the title compound has a new type of

copper-antimony-sulfide layers. The $(en)_{0.5}Cu_2SbS_3$ and $(C_2N_2H_{10})_{0.5}Cu_2SbS_3$ compounds both have layers with the same atomic composition of $[Cu_2SbS_3]$, however, the connection of $[CuS_3]$ triangle and $[SbS_3]$ pyramid is different from that in the title compound. Furthermore, the Cu atoms in $(en)_{0.5}Cu_2SbS_3$ and $(C_2N_2H_{10})_{0.5}Cu_2SbS_3$ are all coordinated to three S atoms, while there exist two kinds of Cu coordination environments (CuS_4 and CuS_3) in KCu_2SbS_3. The nearest Cu−Cu distance in the title compound is beyond 3 Å, which is longer than those in $(en)_{0.5}Cu_2SbS_3$ (2.674 Å) and $(C_2N_2H_{10})_{0.5}Cu_2SbS_3$ (2.666 Å).

Powder XRD and Optical Absorption

The powder XRD pattern of the crystal sample was collected to check the phase purity. The pattern of the sample matches well with that calculated from the single-crystal XRD data of KCu_2SbS_3, and no extra peak was observed (Fig. 2). The diffraction peak at 2ϑ = 9.520° corresponds to the (001) planes,
its high intensity implies the crystal orientation growth along the *ab* plane.

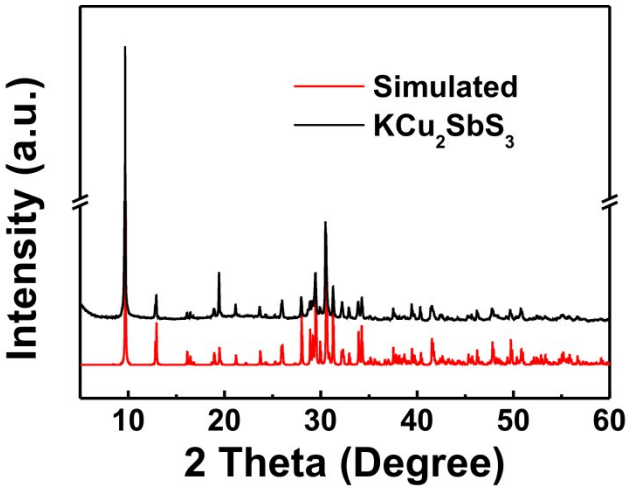

Fig. 2 Powder X-ray diffraction pattern of the KCu_2SbS_3 compound. The simulated pattern was obtained by the *CrystalMaker* program.

The optical properties of KCu_2SbS_3 have been investigated using UV-Vis-NIR diffuse-reflectance spectroscopy (Fig. 3). KCu_2SbS_3 shows an intense optical absorption covering visible and near-infrared light. A sharp absorption edge appears at the wavelength around 800 nm. The band gap energy of KCu_2SbS_3 has been obtained by plotting $(\alpha h\upsilon)^2$ *vs.* $h\upsilon$ for direct band gap (α = absorbance, h = Planck's constant, and υ = frequency) and extrapolating the linear part of the spectrum in the band edge region. The estimated direct band gap is 1.7 eV (as shown in the inset of Fig. 3), suggesting that the KCu_2SbS_3 is a semiconductor with a narrow band gap. The indirect band gap estimated by plotting $(\alpha h\upsilon)^{1/2}$ *vs.* $h\upsilon$ is 1.05 eV, which do not correspond with the color of the compound (as shown in Fig.S2 in ESI). Remarkably, the direct band gap energy of the KCu_2SbS_3 compound is similar to that of the Cu_3SbS_3 (1.84 eV),[26] and $Cu_{12}Sb_4S_{13}$ (1.72 eV),[16] indicating similar electronic band structure. Interestingly, the band gap energy of KCu_2SbS_3 compound is smaller than the reported value for K_2CuSbS_3 (2.2 eV).[29] From the point view of crystal structure, the main

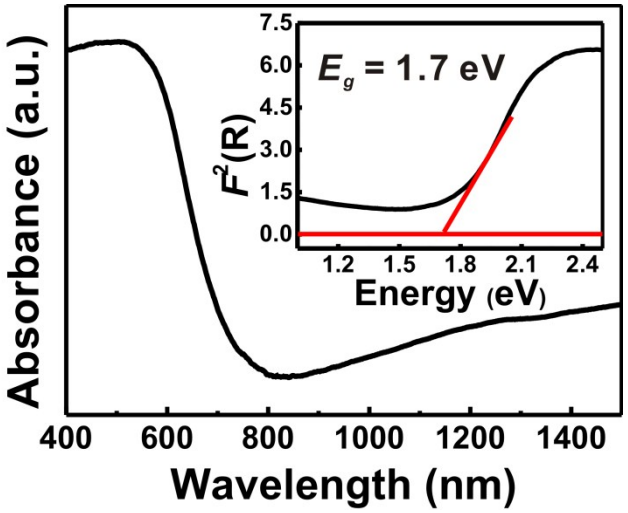

Fig. 3 Ultraviolet-visible-near-infrared (UV-vis-NIR) absorption spectrum of the KCu_2SbS_3 sample. Inset: Plot of $(\alpha h\upsilon)^2$ *vs.* $h\upsilon$ for the absorption spectrum

difference of the two compounds is the presence of $[CuS_4]^{7-}$ tetrahedra in the KCu_2SbS_3 compound, implying the $[CuS_4]^{7-}$ tetrahedra play an important role in narrowing the band gap energy.

Photoelectric Properties and Hall Effect

As mentioned above, the CAS system can provide potential materials for solar energy applications. In addition, the band gap energy of KCu_2SbS_3 is in the optimized solar absorption range (1.2~1.8 eV). Therefore, the title compound should be a good absorber. The photoelectric response properties of the KCu_2SbS_3 were measured under visible light irradiation (cutoff: 420 nm) at room temperature (Fig. 4). A device was constructed by connecting two pieces of Cu foil on the KCu_2SbS_3 pellet (Fig. 4a inset). The current−voltage (I–V) curve of the device is depicted in Fig. 4a. A significant enhancement of the current density under irradiation (8.2 $\mu A/cm^2$ at 10 V), comparing to the dark current (4.5 $\mu A/cm^2$ at 10 V), was observed. Therefore, the photocurrent density of KCu_2SbS_3 compound is 3.7 $\mu A/cm^2$, indicating good photoelectric response properties of the compound. This performance is as well as those of materials such as $CuSbS_2$ in some reports.[43-45] Low current states (light off) and high current states (light on) were observed in the on/off photocurrents measurements at a bias voltage of 10 V (Fig. 4b). The switching is steady and reversible with an "on" state of 8.7 $\mu A/cm^2$ and "off" state of 6.1 $\mu A/cm^2$, implying good potential for application as a photosensitive switch.

The Hall effect measurement of the sample was taken and the resistivity-field curve is shown in Fig.S3 in ESI. The slope of the resistivity-field curve is positive which indicates a *p*-type semiconductor. The charge carrier concentration calculated by $n=1/R_He$ is about 7×10^{16} cm^{-3}, and the carrier mobility is 66.1 $cm^2/V\cdot s$.

Thermal Investigation

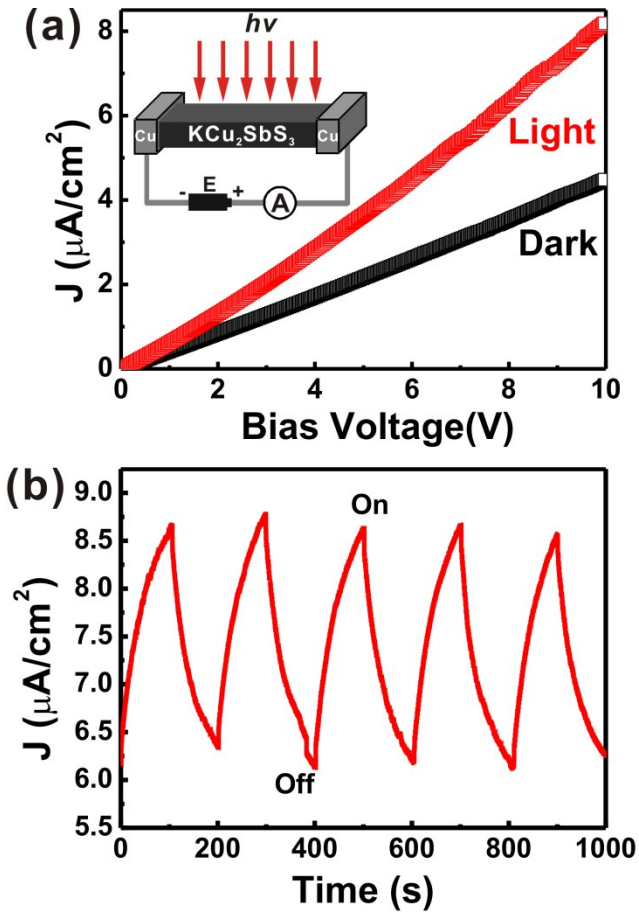

Fig. 4 (a) Photoelectric response of KCu_2SbS_3 and (b) On–off curve at a bias voltage of 10 V.

The thermal stability of KCu_2SbS_3 was probed by differential scanning calorimetry (DSC) and thermogravimetry (TG). The DTA-TG curves are shown in Fig. S4 in ESI. A sharp endothermic peak appears at 421 °C which is attributed to melt and decomposition of the compound. TG curve shows slight weight loss (0.6%) of the compound during heating process.

Electronic Band Structure Calculation

The band structure of KCu_2SbS_3 is shown in Fig. 5a. The valence band maximum and conduction band minimum are both located at *Γ*(0,0,0) with a band gap energy of 1.37 eV. Therefore, the title compound is a direct gap semiconductor. Fig. 5b shows the total density of states (DOS) and the contribution from Cu, Sb, S and K. The Cu 3*d*, Sb 5*p* and S 3*p* orbitals are highly hybridized in the region from −4 eV to the Fermi level caused by the formation of Cu–S and Sb–S bonds (Fig. S5a in ESI). The $5s^2$ lone pairs of Sb atoms are localized between −10 eV and −8 eV (Fig. S5b in ESI), which implies a strong interaction between Cu and Sb.[29] Near the valence band maximum are mainly the Cu 3*d* states. All the Cu, Sb, and S states contribute to construction of the conduction band. The S and Sb states have almost the same DOS which is higher than that of the Cu states.

In comparison with K_2CuSbS_3, KCu_2SbS_3 has smaller band gap energy (2.2 eV for K_2CuSbS_3 and 1.7 eV for KCu_2SbS_3). The main difference between the two compounds is the presence of $[CuS_4]^{7-}$ tetrahedra in the title compound. To understand the origin, the partial DOS of the four independent Cu atoms in the title compound were calculated and are shown in Fig. 6. Obviously, the Cu(3) and Cu(4) in the tetrahedral geometries have higher DOS than that of Cu(1) and Cu(2) in the triangle geometries near the valence band maximum. Therefore, the $CuS_4]^{7-}$ tetrahedra play an important role in constructing the valence band and narrowing the band gap. As shown in Fig. S6 in ESI, the DOS near the valence band maximum are mainly contributed by the d_{xy}, d_{yz}, d_{xz} orbitals of 4-fold coordinated Cu(3) and Cu(4). This can be explained by the ligand field theory (LFT). Since Sb is located at the fourth coordination site of 3-fold coordinated Cu atoms in both compounds, it can be regarded as another 4-fold coordination ligand of the Cu atoms (shown as $[CuSbS_3]$ tetrahedra). According to LFT, the splitting energy (Δ_t) of a tetrahedral field is affected by the interactions between electrons in the *d* orbitals of the center atom and those in the ligands. Compared with the tetrahedron $[CuSbS_3]$ in both K_2CuSbS_3 and KCu_2SbS_3, the tetrahedron CuS_4 in KCu_2SbS_3 has a larger Δ_t because of S is a stronger ligand, resulting in the shorter Cu–S bond length than the Cu···Sb distance. The stronger interaction leads to a larger separation between the *e* and t_2 orbitals of the Cu atom. The crystal field

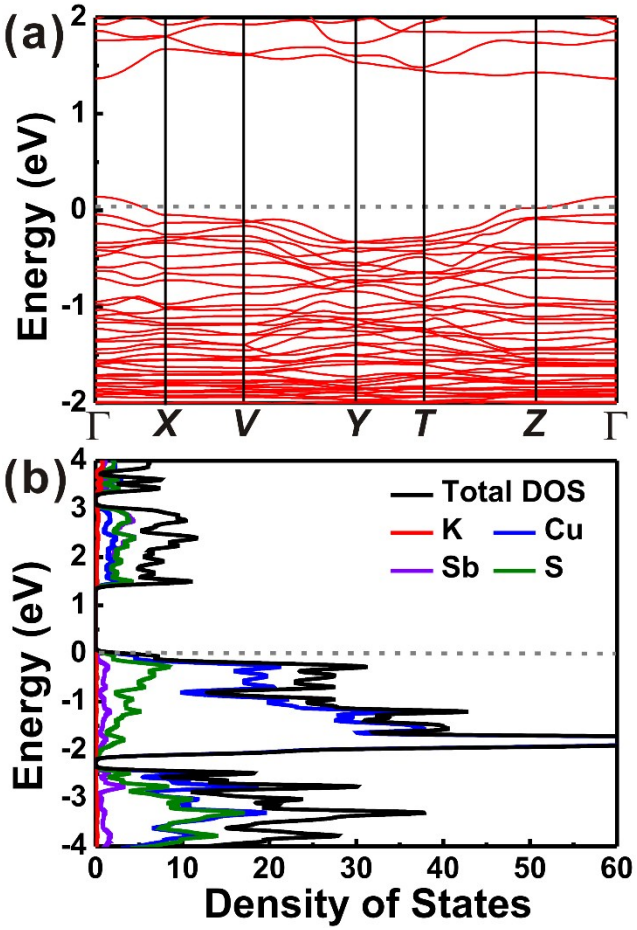

Fig. 5 (a) Electronic band structure of KCu_2SbS_3. (b) The total and selected partial DOS of KCu_2SbS_3

effect causes the rise of the valence band maximum and thus a reduction of the band gap in KCu_2SbS_3.

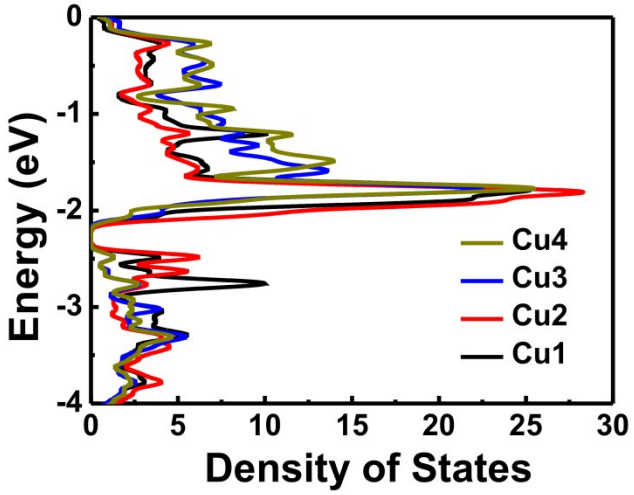

Fig. 6 Partial DOS of Cu atoms in different coordination environments in KCu_2SbS_3.

Conclusions

In summary, a new layered compound KCu_2SbS_3 has been successfully synthesized *via* a facile reactive flux approach. This compound, which consists of $[Cu_2SbS_3]^-$ layers stacking along [001] with K^+ intercalated between layers, crystallizes in the triclinic space group $P\bar{1}$. The $[Cu_2SbS_3]^-$ layers are composed of two single distorted graphene-like layers connected *via* interlayer Cu–S bonding and Cu···Sb intercalation. The UV-Vis-NIR absorption spectrum of the compound shows a band gap of 1.7 eV of the compound. First-principles calculations reveal that the compound is a direct gap semiconductor. The valence band and conduction band are mainly contributed by Cu-3*d*-S-3*p* orbitals, and Sb-5*s*-S-3*p* orbitals, respectively. This compound was fabricated into a device that exhibits notable photoelectric behavior (light on = 8.2μA/cm^2, light off = 4.5 μA/cm^2 at 10 V), suggesting its potential for applications as photoelectric switches.

Acknowledgements

Financial support from 863 Program of China (Grant no. 2011AA050505), the NSF of China (Grants nos. 91122034, 51125006, 51121064, 61376056, 51402341), the CAS/SAFEA International Partnership Program for Creative Research Teams, "Strategic Priority Research Program (B)" of the Chinese Academy of Sciences (Grants XDB04040200) and Chinese Academy of Sciences (Grants nos. KJCX2-EW-W11, KGZD-EW-303) are acknowledged.

Notes and references

1 K.Zweibel, J.Mason, V. Fthenakis, *Sci. Am.* 2008, ***289***, 64-73.
2 F. Kessler and D. Rudmann, *Sol. Energy* 2004, ***77***, 685-695.
3 X. Mathew, J. P. Enriquez, A. Romeo and A. N. Tiwari, *Sol. energy*, 2004, **77**, 831-838.
4 K. Otte, L. Makhova, A. Braun and I. Konovalov, *Thin Solid Films*, 2006, **511**, 613-622.
5 J. Britt and C. Ferekides, *Appl. Phys. Lett.*, 1993, **62**, 2851.
6 X. Wu, *Sol. energy*, 2004, **77**, 803-814.
7 M. A. Green, K. Emery, Y. Hishikawa and W. Warta, *Prog. Photovoltaics Res. Appl.*, 2010, **18**, 346-352.
8 P. Jackson, D. Hariskos, E. Lotter, S. Paetel, R. Wuerz, R. Menner, W. Wischmann and M. Powalla, *Prog. Photovoltaics Res. Appl.*, 2011, **19**, 894-897.
9 B. Shin, O. Gunawan, Y. Zhu, N. A. Bojarczuk, S. J. Chey and S. Guha, *Prog. Photovoltaics Res. Appl.*, 2013, **21**, 72-76.
10 H. Katagiri, K. Jimbo, S. Yamada, T. Kamimura, W. S. Maw, T. Fukano, T. Ito and T. Motohiro, *Appl. Phys. Express*, 2008, **1**, 041201.
11 J. T. Dufton, A. Walsh, P. M. Panchmatia, L. M. Peter, D. Colombara and M. S. Islam, *Phys. Chem. Chem. Phys.*, 2012, **14**, 7229-7233.
12 C. Yan, Z. Su, E. Gu, T. Cao, J. Yang, J. Liu, F. Liu, Y. Lai, J. Li and Y. Liu, *RSC Adv.*, 2012, **2**, 10481-10484.
13 B. Yang, L. Wang, J. Han, Y. Zhou, H. Song, S. Chen, J. Zhong, L. Lv, D. Niu and J. Tang, *Chem. Mater.*, 2014, **26**, 3135-3143.
14 S. Suehiro, K. Horita, M. Yuasa, T. Tanaka, K. Fujita, Y. Ishiwata, K. Shimanoe and T. Kida, *Inorg. chem.*, 2015, **54**, 7840-7845.
15 Y. C. Choi, E. J. Yeom, T. K. Ahn and S. I. Seok, *Angew. Chem. Int. Ed.,* 2015, **54**, 4005-4009.
16 J. van Embden, K. Latham, N. W. Duffy and Y. Tachibana, *J. Am. Chem. Soc.*, 2013, **135**, 11562-11571.
17 H.O. Stephan and M. G. Kanatzidis, *J. Am. Chem. Soc.*, 1996, **118**, 12226-12227.
18 Q. Zhang, I. Chung, J. I. Jang, J. B. Ketterson and M. G. Kanatzidis, *J. Am. Chem. Soc.*, 2009, **131**, 9896-9897.
19 H.O. Stephan and M. G. Kanatzidis, *Inorg. Chem.*, 1997, **36**, 6050-6057.
20 K.S. Choi and M. G. Kanatzidis, *Inorg. Chem.*, 2000, **39**, 5655-5662.
21 M. Schaefer, R. Staehler, W. R. Kiebach, C. Naether and W. Bensch, *Z. Anorg. Allg. Chem.*, 2004, **630**, 1816-1822.
22 R. Staehler, B. D. Mosel, H. Eckert and W. Bensch, *Angew. Chem. Int. Ed.*, 2002, **41**, 4487-4489.
23 R. Staehler and W. Bensch, *Eur. J. Inorg. Chem.*, 2001, **2001**, 3073-3078.
24 M. Schaefer, D. Kurowski, A. Pfitzner, C. Näther, Z. Rejai, K. Möller, N. Ziegler and W. Bensch, *Inorg. Chem.*, 2006, **45**, 3726-3731.
25 J. Zhou, G.-Q. Bian, Q.-Y. Zhu, Y. Zhang, C.-Y. Li and J. Dai, *J. Solid State Chem.*, 2009, **182**, 259-264.
26 P. Maiello, G. Zoppi, R. W. Miles, N. Pearsall and I. Forbes, *Sol. Energy Mater. Sol. Cells*, 2013, **113**, 186-194.
27 K. Ramasamy, H. Sims, W. H. Butler and A. Gupta, *Chem. Mater.*, 2014, **26**, 2891-2899.
28 J. E. Jerome, G. L. Schimek, G. W. Drake and J.W. Kolis, *Eur. J. Solid State Inorg. Chem.*, 1996, **33**, 765-782.
29 B. Deng, G. H. Chan, D. E. Ellis, R. P. Van Duyne and J. A. Ibers, *J. Solid State Chem.*, 2005, **178**, 3169-3175.
30 A. V. Powell, S. Boissière and A. M. Chippindale, *J. Chem.Soc., Dalton Trans.*, DOI: 10.1039/b005111j, 4192-4195.
31 A. V. Powell, R. Paniagua, P. Vaqueiro and A. M. Chippindale, *Chem. Mater.*, 2002, **14**, 1220-1224.

32 V. Spetzler, H. Rijnberk, C. Näther and W. Bensch, *Z. Anorg. Allg. Chem.*, 2004, **630**, 142-148.
33 V. Spetzler, C. Nather and W. Bensch, *Inorg. Chem.*, 2005, **44**, 5805-5812.
34 K. Ramasamy, H. Sims, W. H. Butler and A. Gupta, *J. Am. Chem. Soc.*, 2014, **136**, 1587-1598.
35 G. Sheldrick, University of Göttingen, Germany, 1997.
36 G. Kortüm, W. Braun and G. Herzog, *Angew. Chem.*, 1963, **75**, 653-661.
37 G. Kortüm, W. Braun and G. Herzog, *Angew. Chem. Int. Ed.*, 1963, **2**, 333-341.
38 P. Blaha, K. Schwarz, G. Madsen, D. Kvasnicka and J. Luitz, Technische Universität Wien: Wien, Austria, 2001.
39 J. P. Perdew, K. Burke and M. Ernzerhof, *Phys. Rev. lett.*, 1996, **77**, 3865.
40 P. E. Blöchl, *Phys. Rev. B*, 1994, **50**, 17953.
41 S. A. Sunshine, D. Kang and J. A. Ibers, *J. Am. Chem. Soc.*, 1987, **109**, 6202-6204.
42 M. G. Kanatzidis, *Chem. Mater.*, 1990, **2**, 353-363.
43 Y. Rodrıguez-Lazcano, M. Nair and P. Nair, *J. Cryst. Growth*, 2001, **223**, 399-406.
44 C. Garza, S. Shaji, A. Arato, E. P. Tijerina, G. A. Castillo, T. D. Roy and B. Krishnan, *Sol. Energy Mater. Sol. Cells*, 2011, **95**, 2001-2005.
45 45. L. Shi, Y. Li, C. Wu and Y. Dai, *J. Alloys Compd.*, 2015, **648**, 507-511.
46 X. Zhang, Y. Liu, G. Zhang, Y. Wang, H. Zhang and F. Huang, *ACS Appl. Mater. Interfaces*, 2015, **7**, 4442-4448.
47 X. Zhang, Q. Wang, Z. Ma, J. He, Z. Wang, C. Zheng, J. Lin and F. Huang, *Inorg. chem.*, 2015, **54**, 5301-5308.
48 G. Zhang, B. Zhang, H. Chen, X. Zhang, C. Zheng, J. Lin and F. Huang, *J. Alloys Compd.*, 2014, **591**, 6-10.

The new layered KCu_2SbS_3 was synthesized *via* a facile reactive flux method. The compound, which crystal structure features $[Cu_2SbS_3]^-$ layers packing along [001], possesses a direct-transition band gap of 1.7 eV. Photoelectric measurement demonstrates the potential for applications for photovoltaic devices.